Applied Physics Letters

Monolithic on-chip mid-IR methane gas sensor with waveguide-integrated detector

Cite as: Appl. Phys. Lett. **114**, 051103 (2019); https://doi.org/10.1063/1.5053599
Submitted: 23 August 2018 . Accepted: 20 January 2019 . Published Online: 07 February 2019

P. Su, Z. Han, D. Kita, P. Becla, H. Lin, S. Deckoff-Jones, K. Richardson, L. C. Kimerling, J. Hu, and A. Agarwal

AIP Publishing

Applied Physics Letters ARTICLE scitation.org/journal/apl

Monolithic on-chip mid-IR methane gas sensor with waveguide-integrated detector

Cite as: Appl. Phys. Lett. **114**, 051103 (2019); doi: 10.1063/1.5053599
Submitted: 23 August 2018 · Accepted: 20 January 2019 ·
Published Online: 7 February 2019

P. Su,[1,a)] Z. Han,[1] D. Kita,[1] P. Becla,[2] H. Lin,[1] S. Deckoff-Jones,[1] K. Richardson,[3] L. C. Kimerling,[1] J. Hu,[1,4] and A. Agarwal[1,4]

AFFILIATIONS

[1]Department of Materials Science and Engineering, Massachusetts Institute of Technology, Cambridge, Massachusetts 02139, USA
[2]CapeSym, Natick, Massachusetts 01760, USA
[3]CREOL, The College of Optics and Photonics, University of Central Florida, Orlando, Florida 32816, USA
[4]Materials Research Laboratory, Massachusetts Institute of Technology, Cambridge, Massachusetts 02139, USA

[a)]**Author to whom correspondence should be addressed**: peterxsu@mit.edu.

ABSTRACT

We demonstrate a monolithic waveguide sensor integrated with a detector on-chip for mid-infrared absorption spectroscopic sensing. The optical sensing element comprises a chalcogenide glass spiral waveguide, and the detector is a PbTe photoconductor integrated directly with the chalcogenide waveguide. The limit of detection of the sensor for methane gas was experimentally assessed to be 1% by volume. Further optimization of the fabrication process and normalization of the laser power fluctuations should result in a maximum sensitivity of 330 ppmv.

The ability to determine the chemical composition of or the presence of a chemical in liquid and gaseous mixtures is important for many fields, such as industrial process monitoring, environmental monitoring, forensics, and medicine and biology. One method widely used to determine chemical compositions is optical absorption spectroscopy, which is typically performed in the infrared region of the electromagnetic spectrum where many chemicals have unique absorption spectra.[1] The current equipment used to measure these spectra uses free-space optics that are bulky and expensive, but integrated photonics promises the ability to perform the same analysis with chips that are significantly smaller and that can be mass-produced via techniques similar to those used in the electronics industry.

These chips can generally be broken down into three main constituent parts: the light source, the sensing element, and the detector. Previous work has focused individually on the sensing element and the detector. In the near-infrared, spectroscopic detection of molecules relies on tracing their vibrational overtone absorption. The approach has been implemented using on-chip waveguides[2–7] and resonators.[8–10] Extending the working wavelength of these sensing elements to the mid-infrared (mid-IR), where strong and unique spectroscopic features reside, promises significantly enhanced selectivity and sensitivity,[11] and this has been realized using various material systems including silicon,[12–15] germanium,[16] silicon-germanium,[17] silicon nitride,[18] III–V semiconductors,[19] and chalcogenides.[20–23] Nevertheless, these proof-of-concept sensors still use off-chip light sources and detectors, compromising the benefits of photonic integration.

In this paper, we demonstrate a mid-IR waveguide sensor monolithically integrated with an on-chip detector on a silicon platform. In addition to being a critical step towards a fully integrated chip-scale sensing system, waveguide integrated detectors also offer reduced noise due to decreased size and increased speed.[24,25] Our device borrows elements from our previous work on spiral chalcogenide glass waveguide sensors[22] and waveguide-integrated PbTe detectors.[25,26] PbTe provides a monolithic integration capability that represents a major advantage over previously demonstrated mid-IR waveguide-integrated photodetectors,[27–30] which mostly rely on hybrid bonding or transfer of the active detector material. The use of chalcogenide glass, a well-known Kerr medium, as the sensor material also foresees seamless integration of the sensing element and the detector with on-chip nonlinear sources to enable broadband spectroscopic interrogation.[31]

The design of our sensor is schematically shown in Fig. 1. The sensing element is a $Ge_{23}Sb_7S_{70}$ (GeSbS) chalcogenide glass

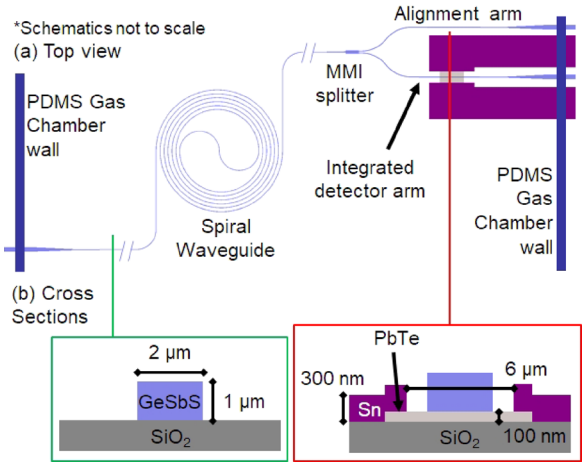

FIG. 1. Schematics (not to scale) of the (a) top view and (b) cross-sectional views of the sensor with a spiral chalcogenide waveguide as the sensing element and a PbTe detector integrated directly underneath the chalcogenide waveguide. The waveguide cross-section is 2 μm wide by 1 μm thick, while the PbTe detector is 100 nm thick and 40 μm long with a 300 nm thick Sn contact on top of the PbTe detector with a contact spacing of 6 μm. The PDMS gas chamber wall only touches the waveguides when they have a cross-section of 15 μm wide by 1 μm thick.

spiral waveguide with a cross-section of 2 μm wide by 1 μm thick, providing single mode waveguiding at the absorption peak of methane at a 3.31 μm wavelength, as shown in Fig. 2. The spiral offers a long interaction length (5 mm) of light with the environment within a small footprint (550 μm by 550 μm), and the minimum bend radius is 100 μm, so the bending loss is negligible. (Lumerical simulations show 10^{-4} dB/cm, or 10^{-6} dB per 90° bend, of bending loss for the 100 μm minimum bend radius.) The gaseous analyte, composed of methane mixed with nitrogen, is transported to the spiral via a polydimethylsiloxane (PDMS) microfluidic channel. To prevent the PDMS microfluidic chamber wall from absorbing much of the guided light where it touches the waveguide, the input and output waveguide widths are adiabatically increased from 2 μm within the chamber to 15 μm as it approaches the PDMS chamber wall to reduce modal overlap with the elastomer and therefore reduce parasitic optical absorption. Light from the spiral sensing element is split using a multimode interferometer to an alignment waveguide and a waveguide with the integrated detector. The integrated detector comprises a 40 μm long PbTe photoconductive layer directly beneath the waveguide.

To fabricate our sensor, we started with a silicon substrate with a 3 μm thermally grown oxide. A 100 nm PbTe film and then a 300 nm thick Sn contact layer are deposited via thermal evaporation[32] and patterned using photolithography and lift-off. The GeSbS layer was then deposited and patterned using an electron-beam-lithography-based liftoff procedure.[33] The wafer was then cleaved to create the input and output waveguide facets, resulting in a chip of approximately 1 cm by 1 cm in size. The PDMS microfluidic chamber was prepared using replica molding and subsequently attached to the chip through plasma bonding to complete the sensor fabrication.

The gas sensing capabilities of the integrated spiral sensor and the PbTe detector were measured using the setup shown in Fig. 3. Light of 3.31 μm wavelength from a tunable mid-IR laser (wavelength tunable from 2.5 to 3.8 μm with a 5 nm linewidth, Firefly, M Squared, Ltd.) is modulated with a chopper at 1 kHz and edge-coupled to the input waveguide via an aspheric lens. Light from the alignment arm of the sensor is coupled via another lens to a cryogenically cooled InSb focal plane array to facilitate alignment. The gas flows of methane and nitrogen carrier gas are regulated using mass flow controllers to achieve different concentrations of methane in the PDMS gas chamber. The integrated PbTe detector is biased using a constant 100 μA current (from a Keithley 6220 current source), and the voltage across the detector is passed to a lock-in amplifier (SR810, Stanford Research Systems) synchronized with the modulation frequency of the chopper. In our experiments, the lock-in time constant is fixed at 1 s, corresponding to an effective noise bandwidth of 0.078 Hz.[34]

The integrated detector signal was monitored under a flow of pure nitrogen for 30 s as a baseline reference, followed by 30 s measurements at different concentrations of methane with a balance of nitrogen. The signal with methane was normalized to the signal under pure nitrogen to obtain the transmittance. The sensor follows Beer's law, which is given by the following equation:

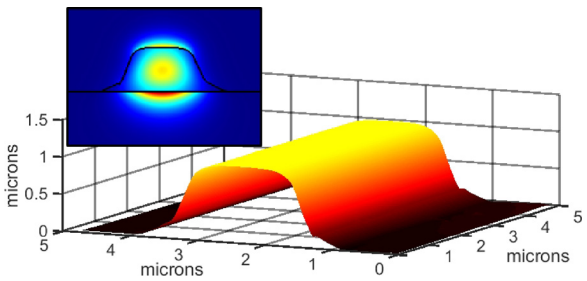

FIG. 2. AFM scan, taken in tapping mode using an Asylum Research Cypher ES AFM and Olympus AC55TS probes, of a section of the waveguide. The average RMS roughness of the sidewall, which slopes 25° away from vertical, calculated from the scan is 2.3 nm. The inset shows the fundamental TM mode simulated using a mode solver. The confinement factor of this mode in the gas is 12.5%.

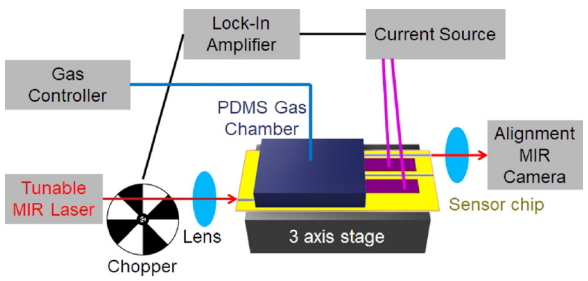

FIG. 3. Schematic of the sensor characterization setup. Modulated 3.31 μm light is coupled to the sensor chip, on top of which is a PDMS gas chamber that can be filled with variable concentrations of methane. The detector is biased with a constant current, and the voltage across the detector is measured by a lock-in amplifier locked into the modulation frequency of the light.

$$T = \frac{V_{CH_4}}{V_{no\,CH_4}} = \exp(-\alpha \Gamma L C), \quad (1)$$

where T is the transmittance, V_{CH_4} is the detector signal under the methane-nitrogen mixture, $V_{no\,CH_4}$ is the detector signal under pure nitrogen, α is the absorbance of pure methane at atmospheric pressure, Γ is the confinement factor in the gas (which is 12.5% based on our modal simulation), L is the length of the sensing element, and C is the methane volumetric concentration. Figure 4 plots the measured modal absorption coefficient ($\Gamma\alpha C$) calculated using Beer's law versus the methane concentration. Each concentration was measured three times to obtain the average and standard error. The response of the sensor agrees well with the fit calculated from Beer's law.

The limit of detection (LOD) of the sensor can be determined by the following equation:

$$LOD = \frac{NEA \cdot SNR}{\alpha \Gamma L}, \quad (2)$$

where NEA is the noise-equivalent absorbance and SNR is the signal-to-noise ratio. We use the commonly adopted 3-σ criterion, giving an SNR of 3. For our sensor, the detector noise was measured to be 8.13 $\mu V/Hz^{1/2}$, while the detector signal under pure nitrogen was measured to be 1.09 mV. This results in a LOD of 3.5 vol. %/$Hz^{1/2}$. Our measurement was performed using a noise bandwidth of 0.078 Hz; so, the minimum detectable concentration is 1 vol. %.

However, this is not the best sensitivity that can be expected from an integrated sensing element and detector. There are two primary considerations that govern the minimum detectable concentration: the waveguide transmission loss, which changes the ideal length of the spiral, and the detector noise.

The waveguide transmission loss was measured using the cutback method with several spiral waveguides of different lengths fabricated on the same chip. Using the shortest spiral as the baseline, the relative loss versus the relative length difference is plotted in Fig. 5. The slope of the best fit line is the transmission loss, which is 8 dB/cm. This transmission loss is higher

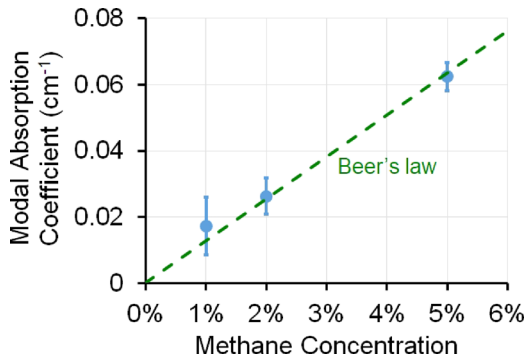

FIG. 4. Sensing results for a 5 mm long spiral sensor. 1 vol. % methane was experimentally measured. Further optimization of the fabrication process and normalization of the laser power fluctuations should result in a maximum sensitivity of 330 ppmv.

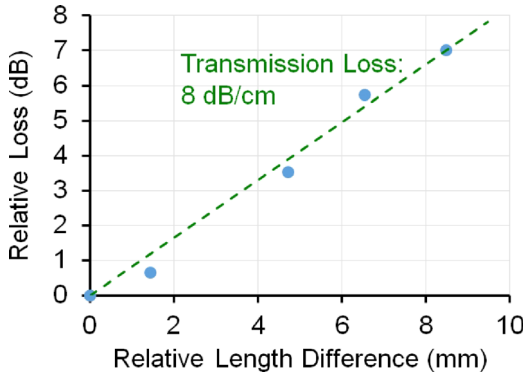

FIG. 5. Relative loss versus length difference for spirals of various lengths. The slope of the best-fit line gives the estimated transmission loss of the waveguides of 8 dB/cm.

than that in other works with chalcogenide glass waveguides, with Du *et al.* being able to achieve 0.5 dB/cm loss at 1550 nm.[35] The higher loss in this work is believed to be due to accumulated organic contamination from the fabrication protocol (being the third step in a multi-step process) and not roughness, since the average RMS sidewall roughness measured via AFM (2.3 nm) is lower than other waveguides fabricated using the same method which show lower loss.[36,37] Improving the fabrication to decrease this loss to 0.8 dB/cm would allow an increase in the spiral length by 10 times, while maintaining the power at the integrated detector. This would enhance the detector signal, improving sensitivity by a factor of 10 to 0.35%/$Hz^{1/2}$ or 0.1% (1000 ppmv) at our experimental noise bandwidth.

The noise measured at the detector can also be further decreased. Using a free space InAsSb detector (PDA10PT, Thorlabs), the laser power fluctuation noise was measured using the same effective noise bandwidth of 0.078 Hz, resulting in a noise of 0.20% of the power of the laser. This turns out to be the dominant contributor to our measured noise levels, and eliminating this by simultaneously measuring laser power along with the sensor signal decreases the measured noise to 2.74 $\mu V/Hz^{1/2}$. Combined with the waveguide loss improvement, the minimum detectable concentration becomes 0.12%/$Hz^{1/2}$ or 0.033% (330 ppmv) at our experimental noise bandwidth. The theoretical minimum noise for a photoconductor like PbTe is the Johnson-Nyquist noise level, which is given by the following equation:

$$V_{noise} = \sqrt{4 k_B T R \Delta f}, \quad (3)$$

where k_B is the Boltzmann constant, T is the temperature, R is the resistance of the detector, and Δf is the noise bandwidth. The Johnson-Nyquist noise level of our 24 kΩ detector at room temperature is 20 nV/$Hz^{1/2}$, still several orders of magnitude smaller than the remaining noise measured. Further work is ongoing to characterize and understand the sources of the remaining noise to improve sensitivity.

In conclusion, we have demonstrated a fully integrated sensing element and detector on-chip for mid-infrared absorption

spectroscopic sensing at room temperature. The sensor is composed of a spiral waveguide sensing element and a waveguide-integrated PbTe detector. Using methane gas as a model gas, our integrated sensor is able to detect 1% methane at 3.31 μm using a noise bandwidth of 0.078 Hz following the 3-σ criterion. The stability of the sensor is very good, with no apparent drift during measurements. Further improvements to the fabrication process and eliminating laser power fluctuation noise would result in a maximum sensitivity of 330 ppmv, while more work needs to be done to understand and eliminate the remaining noise sources from the detector.

Funding from the DOE-NNSA Grant No. DE-NA0002509 and NSF Award No. 1506605 is gratefully acknowledged. This work made use of the MRSEC Shared Experimental Facilities at MIT, supported by the National Science Foundation under Award No. DMR-1419807.

REFERENCES

[1]A. Schliesser, N. Picqué, and T. W. Hänsch, Nat. Photonics **6**, 440 (2012).
[2]J. Hu, V. Tarasov, A. Agarwal, L. Kimerling, N. Carlie, L. Petit, and K. Richardson, Opt. Express **15**, 2307 (2007).
[3]E. Ryckeboer, R. Bockstaele, M. Vanslembrouck, and R. Baets, Biomed. Opt. Express **5**, 1636 (2014).
[4]W.-C. Lai, S. Chakravarty, X. Wang, C. Lin, and R. T. Chen, Opt. Lett. **36**, 984 (2011).
[5]M.-L. Anne, J. Keirsse, V. Nazabal, K. Hyodo, S. Inoue, C. Boussard-Pledel, H. Lhermite, J. Charrier, K. Yanakata, O. Loreal, J. Le Person, F. Colas, C. Compère, and B. Bureau, Sensors **9**, 7398 (2009).
[6]J. Charrier, M. L. Brandily, H. Lhermite, K. Michel, B. Bureau, F. Verger, and V. Nazabal, Sens. Actuators, B **173**, 468 (2012).
[7]L. Tombez, E. J. Zhang, J. S. Orcutt, S. Kamlapurkar, and W. M. J. Green, Optica **4**, 1322 (2017).
[8]A. Nitkowski, A. Baeumner, and M. Lipson, Biomed. Opt. Express **2**, 271 (2011).
[9]A. Nitkowski, L. Chen, and M. Lipson, Opt. Express **16**, 11930 (2008).
[10]J. Hu, N. Carlie, L. Petit, A. Agarwal, K. Richardson, and L. C. Kimerling, J. Lightwave Technol. **27**, 5240 (2009).
[11]H. Lin, Z. Luo, T. Gu, L. C. Kimerling, K. Wada, A. Agarwal, and J. Hu, Nanophotonics **7**, 393 (2017).
[12]C. J. Smith, R. Shankar, M. Laderer, M. B. Frish, M. Loncar, and M. G. Allen, Opt. Express **23**, 5491 (2015).
[13]Y. Zou, S. Chakravarty, P. Wray, and R. T. Chen, Sens. Actuators, B **221**, 1094 (2015).
[14]V. Singh, P. T. Lin, N. Patel, H. Lin, L. Li, Y. Zou, F. Deng, C. Ni, J. Hu, J. Giammarco, A. P. Soliani, B. Zdyrko, I. Luzinov, S. Novak, J. Novak, P. Wachtel, S. Danto, J. D. Musgraves, K. Richardson, L. C. Kimerling, and A. M. Agarwal, Sci. Technol. Adv. Mater. **15**, 014603 (2014).
[15]Y. Chen, H. Lin, J. Hu, and M. Li, ACS Nano **8**, 6955 (2014).
[16]W. Li, P. Anantha, K. H. Lee, H. D. Qiu, X. Guo, S. C. K. Goh, L. Zhang, H. Wang, R. A. Soref, and C. S. Tan, IEEE Photonics J. **10**, 2201107 (2018).
[17]Q. Liu, J. M. Ramirez, V. Vakarin, X. L. Roux, A. Ballabio, J. Frigerio, D. Chrastina, G. Isella, D. Bouville, L. Vivien, C. A. Ramos, and D. Marris-Morini, Opt. Mater. Express **8**, 1305 (2018).
[18]P. T. Lin, H.-Y. G. Lin, Z. Han, T. Jin, R. Millender, L. C. Kimerling, and A. Agarwal, Adv. Opt. Mater. **4**, 1755 (2016).
[19]M. Sieger, J. Haas, M. Jetter, P. Michler, M. Godejohann, and B. Mizaikoff, Anal. Chem. **88**, 2558 (2016).
[20]V. Mittal, M. Nedeljkovic, D. J. Rowe, G. S. Murugan, and J. S. Wilkinson, Opt. Lett. **43**, 2913 (2018).
[21]P. Ma, D.-Y. Choi, Y. Yu, X. Gai, Z. Yang, S. Debbarma, S. Madden, and B. Luther-Davies, Opt. Express **21**, 29927 (2013).
[22]Z. Han, P. Lin, V. Singh, L. Kimerling, J. Hu, K. Richardson, A. Agarwal, and D. T. H. Tan, Appl. Phys. Lett. **108**, 141106 (2016).
[23]E. Baudet, A. Gutierrez-Arroyo, M. Baillieul, J. Charrier, P. Němec, L. Bodiou, J. Lemaitre, E. Rinnert, K. Michel, B. Bureau, J. L. Adam, and V. Nazabal, Adv. Device Mater. **3**, 23 (2017).
[24]D. Ahn, C. Hong, J. Liu, W. Giziewicz, M. Beals, L. C. Kimerling, J. Michel, J. Chen, and F. X. Kärtner, Opt. Express **15**, 3916 (2007).
[25]Z. Han, V. Singh, D. Kita, C. Monmeyran, P. Becla, P. Su, J. Li, X. Huang, L. C. Kimerling, J. Hu, K. Richardson, D. T. H. Tan, and A. Agarwal, Appl. Phys. Lett. **109**, 071111 (2016).
[26]V. Singh, T. Zens, J. Hu, J. Wang, J. D. Musgraves, K. Richardson, L. C. Kimerling, and A. Agarwal, Sens. Actuators, B **185**, 195 (2013).
[27]N. Hattasan, A. Gassenq, L. Cerutti, J. B. Rodriguez, E. Tournié, and G. Roelkens, IEEE Photonics Technol. Lett. **23**, 1760 (2011).
[28]A. Gassenq, N. Hattasan, L. Cerutti, J. B. Rodriguez, E. Tournié, and G. Roelkens, Opt. Express **20**, 11665 (2012).
[29]M. Muneeb, A. Vasiliev, A. Ruocco, A. Malik, H. Chen, M. Nedeljkovic, J. S. Penades, L. Cerutti, J. B. Rodriguez, G. Z. Mashanovich, M. K. Smit, E. Tourni, and G. Roelkens, Opt. Express **24**, 9465 (2016).
[30]H. Lin, Y. Song, Y. Huang, D. Kita, S. Deckoff-Jones, K. Wang, L. Li, J. Li, H. Zheng, Z. Luo, H. Wang, S. Novak, A. Yadav, C.-C. Huang, R.-J. Shiue, D. Englund, T. Gu, D. Hewak, K. Richardson, J. Kong, and J. Hu, Nat. Photonics **11**, 798 (2017).
[31]Q. Du, Z. Luo, H. Zhong, Y. Zhang, Y. Huang, T. Du, W. Zhang, T. Gu, and J. Hu, Photonics Res. **6**, 506 (2018).
[32]J. Wang, J. Hu, X. Sun, A. M. Agarwal, L. C. Kimerling, D. R. Lim, and R. A. Synowicki, J. Appl. Phys. **104**, 053707 (2008).
[33]L. Zhang, J. Ding, H. Zheng, S. An, H. Lin, B. Zheng, Q. Du, G. Yin, J. Michon, Y. Zhang, Z. Fang, M. Y. Shalaginov, L. Deng, T. Gu, H. Zhang, and J. Hu, Nat. Commun. **9**, 1481 (2018).
[34]"Model SR810 DSP Lock-In Amplifier User Manual" (2005).
[35]Q. Du, Y. Huang, J. Li, D. Kita, J. Michon, H. Lin, L. Li, S. Novak, K. Richardson, W. Zhang, and J. Hu, Opt. Lett. **41**, 3090 (2016).
[36]J. Hu, N.-N. Feng, N. Carlie, L. Petit, A. Agarwal, K. Richardson, and L. Kimerling, Opt. Express **18**, 1469 (2010).
[37]K. Richardson, L. Petit, N. Carlie, B. Zdyrko, I. Luzinov, J. Hu, A. Agarwal, L. Kimerling, T. Anderson, and M. Richardson, J. Nonlinear Opt. Phys. Mater. **19**, 75 (2010).